Bioactive Materials 43 (2025) 550–563

Contents lists available at ScienceDirect

Bioactive Materials

journal homepage: www.keaipublishing.com/en/journals/bioactive-materials

A natural polyphenolic nanoparticle--knotted hydrogel scavenger for osteoarthritis therapy

Qinfeng Ding [a,1], Yitong Wang [a,b,1], Tianyou Wang [c,1], Chengyao Zhang [d,1], Shengbing Yang [e], Lu Mao [f,****], Yiyun Cheng [g,***], Yiwen Li [c,**], Kaili Lin [a,*]

[a] Department of Oral & Cranio-Maxillofacial Surgery, Shanghai Ninth People's Hospital, College of Stomatology, Shanghai Jiao Tong University School of Medicine, National Clinical Research Center for Oral Diseases, Shanghai Key Laboratory of Stomatology & Shanghai Research Institute of Stomatology, Shanghai, 200011, China
[b] Department of Radiology, Shanghai Tenth People's Hospital, Tongji University School of Medicine, Shanghai, 200072, China
[c] College of Polymer Science and Engineering, State Key Laboratory of Polymer Materials Engineering, Sichuan University, Chengdu, 610065, China
[d] Department of Thyroid Oncology, Chongqing University Cancer Hospital, Chongqing, 400030, China
[e] Shanghai Key Laboratory of Orthopaedic Implants, Department of Orthopaedic Surgery, Shanghai Ninth People's Hospital, Shanghai Jiao Tong University School of Medicine, Shanghai, 200011, China
[f] Department of Spine Surgery, Zhongda Hospital, Southeast University, Nanjing, 210009, China
[g] School of Life Science, Shanghai Key Laboratory of Regulatory Biology, East China Normal University, Shanghai, 200241, China

ARTICLE INFO

Keywords:
Osteoarthritis therapy
Tea polyphenol nanoparticle
Antioxidant
Nitric oxide scavenging
pH-responsive release

ABSTRACT

Exploring highly efficient and cost-effective biomaterials for osteoarthritis (OA) treatment remains challenging, as current therapeutic strategies are difficult to eradicate the excessive reactive oxygen species (ROS) and nitric oxide (NO) at damaged sites. Tea polyphenol (TP) nanoparticles (NPs), a nature-inspired antioxidant in combination with 2-(4-Carboxyphenyl)-4,4,5,5-tetramethylimidazoline-1-oxyl-3-oxide (carboxy-PTIO), a NO scavenger, could provide maximized positive therapeutic effects on OA by eradicating both ROS and NO. Notably, this combination not only improves the half-life of the TP monomer and the drug loading efficiency of carboxy-PTIO but also prevents nitrite from being harmful to tissue. Moreover, the protonation ability of carboxy-PTIO allows smart acid-responsive release in response to environmental pH, which provides conditioned treatment strategies for OA. In *in vitro* experiments, TP/PTIO NPs downregulated proinflammatory cytokine release via synergistic removal of ROS and NO and suppression of ROS/NF-κB and iNOS/NO/Caspase-3 signaling. For *in vivo* experiments, NPs were cross-linked with 4-arm-PEG-SH to form an injectable hydrogel system. The release of TP and carboxy-PTIO from the system efficiently prevents cartilage inflammation and damage via similar signaling pathways. Overall, the proposed system provides an efficient approach for OA therapy.

1. Introduction

Osteoarthritis (OA), the main cause of disability in the aging population [1–3], affects more than 20 % of middle-aged and elderly individuals worldwide [2,4,5]. As the most common form of arthritis, OA patients are characterized by morphological and molecular changes in the entire joint that lead to softening, ulceration and loss of articular cartilage [1]. In addition, as a multifactorial and polygenic disease, OA is influenced by proinflammatory genetic and environmental mediators such as overload, trauma, estrogen level, nutritional status, and genetic susceptibility [3,6–9], which may contribute to articular injury, cartilage degeneration, and synovitis [1]. In view of the clinically unclear etiology of OA, current treatment strategies for this disease include nondrug/drug therapy and arthrocentesis [10,11]. However, neither

Peer review under responsibility of KeAi Communications Co., Ltd.
* Corresponding author.
** Corresponding author.
*** Corresponding author.
**** Corresponding author.
E-mail addresses: 101012005@seu.edu.cn (L. Mao), yycheng@mail.ustc.edu.cn (Y. Cheng), ywli@scu.edu.cn (Y. Li), linkaili@sjtu.edu.cn, lklecnu@aliyun.com (K. Lin).
[1] These authors contributed equally to the work.

https://doi.org/10.1016/j.bioactmat.2024.09.037
Received 4 March 2024; Received in revised form 13 September 2024; Accepted 27 September 2024
Available online 11 October 2024

noninvasive and minimally invasive therapies nor irreversible surgical interventions at the late stage can achieve satisfactory results due to the complexity of the joint structure, which leads to difficulty in identifying the specific molecular mechanisms of OA, and a lack of long-lasting but affordable biosafe drugs. From this clinical perspective, new effective and minimally invasive therapies with high efficiency and limited cost are worth exploring.

Controlling endogenous contributory factors might be an effective strategy for OA treatment. The overaccumulation of reactive oxygen species (ROS, byproducts of oxidative phosphorylation) and proinflammatory factors in the OA microenvironment is regarded as the main cause of OA [12]. Excessive ROS oxidize and destroy cartilage homeostasis subsequently, initiating catabolism and ultimately degrading cartilage by inducing chondrocyte inflammation and apoptosis [13]. On the other hand, migrated innate immune cells overproduce proinflammatory factors such as Interleukin-1β (IL-1β), IL-1α,IL-6, and tumor necrosis factor-alpha (TNF-α) [14,15] in the synovial fluid of the intra-articular microenvironment [16], which further activates chondrocytes and initiates the overproduction of nitric oxide (NO) and accumulation of matrix metalloproteinases (MMPs), proteases, and chemokines, resulting in degradation in cartilage [17,18]. Notably, among the factors that cause OA progression, NO is considered the main factor that induces chondrocyte apoptosis [19]. NO accumulates mainly in mitochondria. In addition to being a known inducer of apoptosis, NO also promotes the degradation of cartilage matrix macromolecules (aggrecan, etc.) and increases MMP activity in chondrocytes [20,21]. Research has shown that the accumulation of NO in joints and blood positively correlated with the severity of OA [19,22]. Moreover, immunohistochemical analysis has confirmed the overexpression of inducible nitric oxide synthase (iNOS) in chondrocytes in OA condition [20], while iNOS is an important factor for NO production and proinflammatory cytokine activation [23]. Identifying novel biomaterials that are eligible to control NO production together with ROS generation in inflamed knee joints might lead to more effective and favorable strategies for controlling cartilage degradation and alleviating OA progression.

Natural polyphenols are widely present and have been used as exogenous antioxidative supplements in bioactive foods and medicines aimed at preventing oxidative stress-associated diseases [24–31]. Tea polyphenols (TPs), which are extracted from tea leaves, have satisfactory anti-inflammatory and antioxidative effects and have attracted worldwide attention in the field of biomedical science [32–34]. TP eliminates ROS directly [35], as TP reacts with free radicals such as hydroxyl (HO•), superoxide (O_2•–) and peroxy radicals, as well as nonradicals such as peroxynitrite (OONO-) and hypochlorous acid salt (ClO-) [36,37]. Notably, TP has been proven to clear ROS by entering and enriching mitochondria [38]. Therefore, TP has potential for OA treatment. However, the use of TP monomer in OA treatment has been limited by its half-life of approximately 30 min and limited ability to target NO [39]. Fabricating macromolecular TP materials might help solve this limitation. Macromolecular TP may not only elongate the TP half-life but also serve as a drug carrier to load NO scavengers to exert dual benefits on OA patients. Carboxy-PTIO, a commonly used nitric oxide (NO) scavenger [40], can react with NO to form carboxy-PTI derivatives and produce nitrite or nitrate, thereby eliminating environmental NO. These carboxy-PTI derivatives can further inhibit iNOS, with a 2-fold greater inhibition efficiency than similar inhibitors such as N G-methyl-L-arginine or NG-nitro-L-arginine. However, the nitrite formed after NO scavenging may have biological toxicity potential, which prevents the biological application of carboxy-PTIO. TP can prevent the synthesis of N-nitroso compounds to remove the nitrite produced by the carboxy-PTIO reaction [41]. Therefore, the combined use of macromolecular TP with carboxy-PTIO may provide additional positive therapeutic effects to OA patients through the dual eradication of ROS and NO with limited side effects.

In this study, bioactive low-cost TP nanoparticles (NPs) with extended half-lives were designed by the enzymatic polymerization of TP monomers. Using these TP NPs as a carrier platform, carboxy-PTIO was loaded onto the surface through π-π interactions. Notably, a smart acid-responsive release ability could be present in the system, as the protonation ability of carboxy-PTIO in an acidic microenvironment could weaken the π-π interactions with TP NPs, allowing a controlled release of TP and carboxy-PTIO from the NP system in an acidic OA microenvironment (pH may be 5.5–6.0) [42–45]. In addition, to increase the clinical application of the NP system, polyethylene glycol (PEG), a commonly used lubricant, was proposed for the construction of NPs containing hydrogels for use in slowing cartilage wear and alleviating the progression of OA [46]. In this study, we evaluated the acid response, ROS and NO scavenging ability, drug release ability, micromorphology, gelation behavior, and degradation profile of the TP/PTIO + PEG compound system. An *in vitro* study was performed to determine the cytotoxicity, ROS and NO scavenging ability, anti-inflammatory effects and signaling pathways of the NPs, and an OA mouse model was also adapted to evaluate the therapeutic functions *in vivo*. This study designed a novel NP-based hydrogel system for OA treatment that has synergistic effects on ROS and NO scavenging ability, sustained acid-responsive degradation ability, and controlled release behavior (Scheme 1).

2. Results and discussion

2.1. Fabrication of NPs

The synthesis of tea polyphenols/carboxy-PTIO (TP/PTIO) NPs is illustrated in Fig. 1A. Briefly, TP NPs with excellent drug-carrying capacity were fabricated via a green enzymatic polymerization strategy [32]. This process was relatively fast, with a uniform spherical NP morphology successfully achieved after 6 h, which could be visualized via transmission electron microscopy (TEM) with a diameter of approximately 99.43 ± 1.14 nm (Fig. 1B). Using TP NPs as a carrier, carboxy-PTIO, the NO scavenger was loaded onto TP NPs through π-π interactions to form TP/PTIO NPs (Fig. 1B). The size and zeta potential of the TP NPs changed after carboxy-PTIO loading, indicating successful modification of the NP structure and good stability in aqueous solution (Fig. 1C and D). Additionally, the characteristic peak of carboxy-PTIO appeared for the TP/PTIO NPs, suggesting successful loading of carboxy-PTIO onto the surface of the TP NPs (Fig. 1E). The carboxy-PTIO drug loading efficiency in TP/PTIO NPs was 14.07 % according to the carboxy- PTIO peak in TP/PTIO by HPLC and carboxy-PTIO standard curve (Fig. S12). The structures of the TP/PTIO NPs were evaluated using Fourier transform infrared spectroscopy (FT-IR), and spectra identical to those of the TP NPs were observed, with characteristic peaks at ≈3400 and ≈ 1200 cm−1 corresponding to the O-H group and pyrogallol group [47], respectively (Fig. 1F). In addition, a characteristic PTIO peak appeared at approximately ≈1550 cm-1 in the spectrum of the TP/PTIO NPs, which was attributed to the vibration of the imidazolium ring [48]. This identification was consistent with the X-ray photoelectron spectroscopy (XPS) results (Fig. 1G).

The stability of the NPs was first evaluated in Dulbecco's modified Eagle medium (DMEM) supplemented with 10 % fetal bovine serum (FBS), phosphate-buffered saline (PBS), and H_2O. As shown in Fig. S4, no precipitation or aggregation occurred after 7 days of incubation, indicating a favorable stability of the NPs in physiological media. The stimulus-responsive release behavior was evaluated under a simulated OA microenvironment (pH = 6.0), and physiological conditions (pH = 7.4) were used as controls. The TP/PTIO NPs exhibited an ideal acid-responsive release of carboxy-PTIO, an NO scavenger, under OA conditions (Fig. 1H), suggesting that TP might possess therapeutic potential by downregulating NO levels at OA sites. Moreover, the TP monomer was also released from the NPs persistently over 28 days, indicating a greatly extended half-life (Fig. 1I). Overall, TP/PTIO NPs with controlled release behavior was successfully fabricated, and their

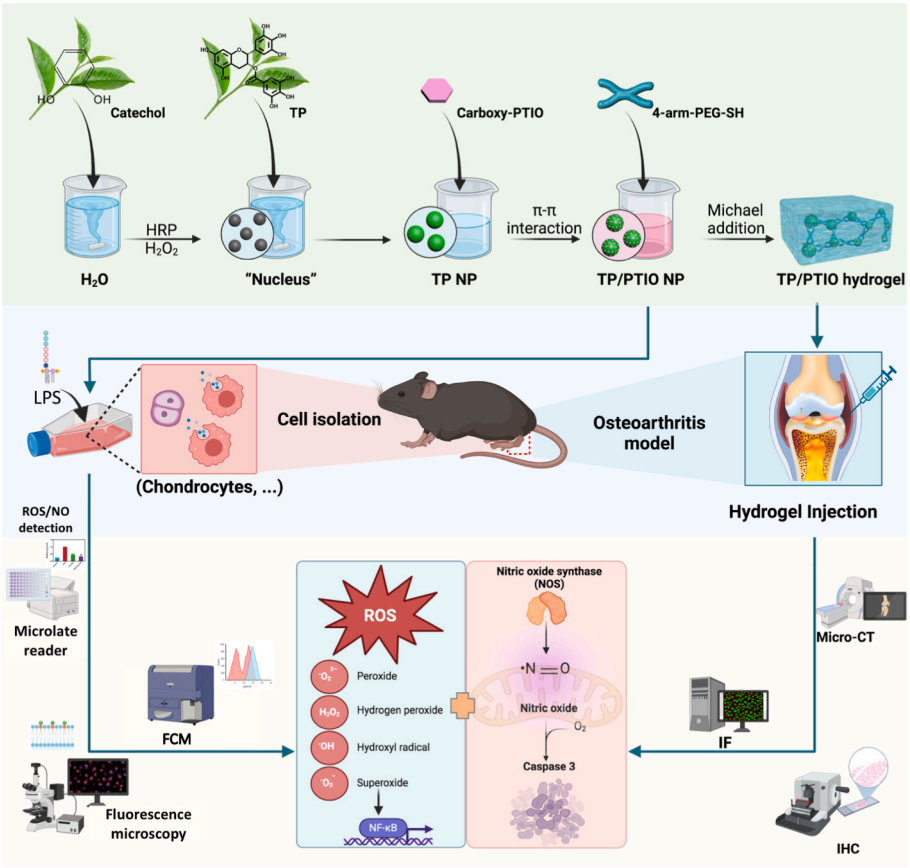

Scheme 1. Schematic illustration of the fabrication of an acid-responsive TP NP-based hydrogel platform for osteoarthritis therapy.

therapeutic effects on OA were subsequently evaluated.

2.2. The anti-inflammatory behaviours of NPs in vitro

Increased levels of proinflammatory mediators are major characteristics in the synovial fluids of end stage OA patients [49,50], while Oxidative stress caused by ROS and NO play a pivotal role in the over activation of the inflammatory responses to produce proinflammatory cytokines and chemokines, leading to cartilage ECM turnover and chondrocytes apoptosis to aggregate OA [49]. Studies have shown that suppressing the expression of ROS associated genes IL-1β and TNF-α [51], MMP-1, -3 and -13 and COX-2, or increasing the expression of [52] exerted chondroprotective effects in chondrocytes and animal models of OA. Besides, currently available therapies for the management of OA also include non-steroidal anti-inflammatory drugs [53], indicating the importance of inflammation control in OA therapy. Therefore, controlling inflammation in OA help achieve the therapeutic action of treating OA.

Due to the extraordinary structural characteristics of the TP/PTIO NPs, we applied them to OA to determine the anti-inflammatory potential of the NPs, as proinflammatory factors accumulated at damaged sites is the main cause of OA. Immune cell infiltration of OA synovial tissue by subpopulations of T cells and activated macrophages correlates with OA disease progression and pain. The innate and acquired immune system plays a key role in the low-grade inflammation found associated with OA [54]. Therefore, Raw cells as a canonical mouse macrophage, has been adapted as a representative of immune cells to simulate the immune responses in OA. Specifically, Raw 264.7 cells were adapted as the representative cells and treated with lipopolysaccharide (LPS, 100 ng/mL) for 24 h, after which TP/PTIO NPs were added and incubated with the cells for another 24 h (Fig. 2A). The internalization and intracellular distribution of TP or TP/PTIO in Raw 264.7 cells were first evaluated by labelling TP or TP/PTIO NPs with Cyanine5.5 amine and visualized under confocal microscopy (Fig. 2B). TP and TP/PTIO NPs entered the cell and distributed evenly in the cytoplasm of Raw 264.7 cell. Both the TP and the TP/PTIO NPs showed satisfactory biocompatibility at concentrations no greater than 80 μg/mL (Fig. 2C). As shown in the Caspase3/7 activity and mitochondrial membrane potential detection assay results and Calcein AM/PI live and dead staining images, TP/PTIO NPs effectively inhibited Raw 264.7 cell apoptosis induced by LPS (Fig. 2C–E). Activated Caspase 3/7 cleaves Poly (ADP-ribose) polymerase (PARP), an important nuclear protein important for cellular differentiation, proliferation, and cellular apoptosis, to yield an 89 kD fragment [55], therefore, we also determined the level of cleaved PARP-1 in Raw 264.7 cells. As expected, TP/PTIO NPs (especially at the concentration 80 μg/mL) eliminated cleaved PARP-1 production caused by LPS in the cells (Fig. S13), which was in line with the caspase 3 activation in cells. A proportion of cleaved PARP-1 protein was found translocated to the cytoplasm (Fig. S13A) after LPS as the protein may combine to the cytoplasm molecules with the assistance of poly (ADP-ribose) (PAR) [55], and this translocation was also significantly eliminated after TP/PTIO NPs supplementation. TP/PTIO also demonstrated more significant anti-cleaved PARP-1 effects than TP NPs (Fig S13). Correspondingly, TP and TP/PTIO NPs suppressed the release of the LPS-upregulated proinflammatory mediators IL-1β, IL-6, TNF-α, and cyclooxygenase-2 (COX-2) in Raw 264.7 cells at both the gene expression level (Fig. 2F–I) and protein production level (Fig. 2J–M).

2.3. ROS scavenging and ROS/NF-κB signaling regulation in vitro

Excessive accumulation of ROS in the local microenvironment is the major risk factor for OA [56]. To verify the free radical clearance ability

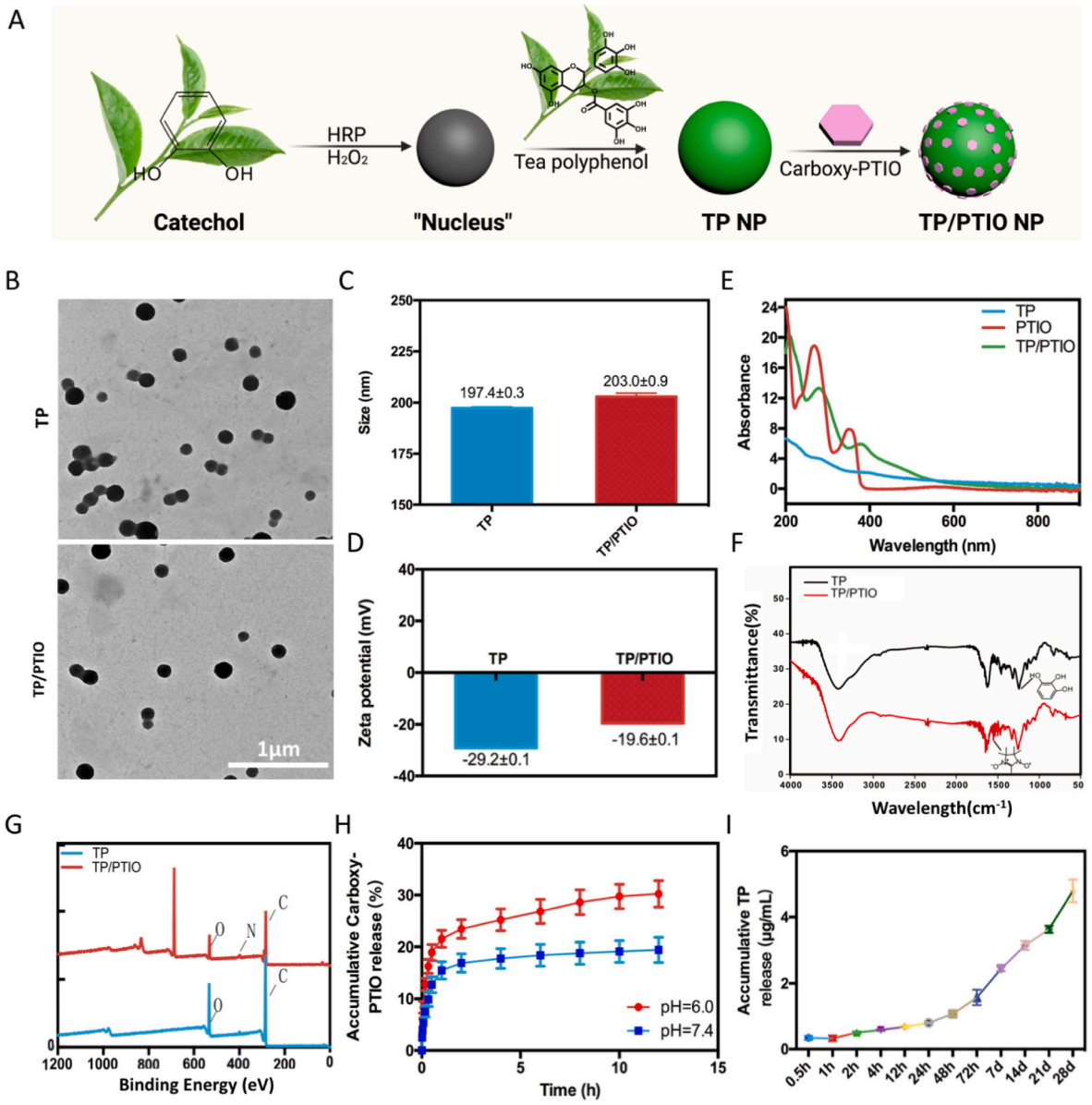

Fig. 1. Fabrication and characterization of TP/PTIO NPs. (A) Synthesis of TP/PTIO NPs. (B) TEM images of synthesized TP and TP/PTIO NPs. (C) and (D) Zeta potential and size of the NPs. (E) Ultraviolet–visible (UV–Vis) spectra of TP, PTIO and the TP/PTIO NPs. (F) FT-IR spectra of TP and the TP/PTIO NPs. (G) XPS analysis of TP and the TP/PTIO NPs. (H) The release ratios of carboxy-PTIO from TP/PTIO NPs at pH 6.0 and 7.4 measured by high-performance liquid chromatography (HPLC). (I) TP released from the TP/PTIO NPs was measured by HPLC.

of the NPs, we determined the radical scavenging abilities of the TP/PTIO NPs. 2,2-diphenyl-1-picrylhydrazyl (DPPH) and 2,2'-azino-bis (3-ethylbenzothiazoline-6-sulfonic acid (ABTS) are the 2 most widely used assays to determine free radical scavenging capacity. After an incubation of 30 min, a scavenge ability of 43.82 ± 0.34 % by TP NPs (TP) and 44.20 ± 0.40 % by TP/PTIO NPs (TP/PTIO) was observed in DPPH assay. Similarly, an ABTS scavenge ability of 34.86 ± 1.39 % by TP and 37.08 ± 1.16 % by TP/PTIO was observed. No significant differences were found between TP and TP/PTIO in DPPH and ABTS assay, which might attribute to the fact that carboxy-PTIO in TP/PTIO targets NO while DPPH and ABTS are sensitive to reactive oxygen species. (Fig. 3A and B). TP/PTIO NPs effectively decomposed into PTIO and TP monomer under cell culture condition (Fig. S6) with an acid responsive characteristics. We next determined whether TP-embedded NPs have antioxidative potential and mediate OA-related inflammation via ROS-related signaling. Hydrogen peroxide (H2O2) was adapted as its the major ROS in redox regulation of biological activities. Both TP and TP/PTIO NPs at a concentration of 80 μg/mL were able to scavenge ROS (induced by H_2O_2) to almost the same extent as the control group, suggesting an ideal antioxidative capacity of the TP and TP/PTIO NPs (Fig. 3D and G). TP and TP-PTIO NPs showed similar scavenging ability with respect to H_2O_2, this may attribute to the fact that carboxy-PTIO is a NO scavenger, which may not response to ROS significantly. Raw 264.7 cells after H_2O_2 treatment were stained with DCFH-DA, a ROS probe, and visualized under fluorescence microscopy (Fig. 3E). Later, the sustained release capacity of TP NPs was further evaluated by incubating TP NPs or TP monomer with H_2O_2 solution which was supplied to the incubation system at regular interval. TP NPs demonstrated the best H_2O_2 controlling ability over time (Fig. S3).

The H_2O_2 generation ability of LPS were evaluated as well. As expected, LPS was able to induce ROS generation in Raw 264.7 cells, while TP-embedded NPs scavenged intracellular ROS (Fig. 3C). ROS induced by LPS was quantified by flow cytometry (Fig. 3F and H). A less mean fluorescence intensity (MFI) was noticed in LPS conditioned cells after

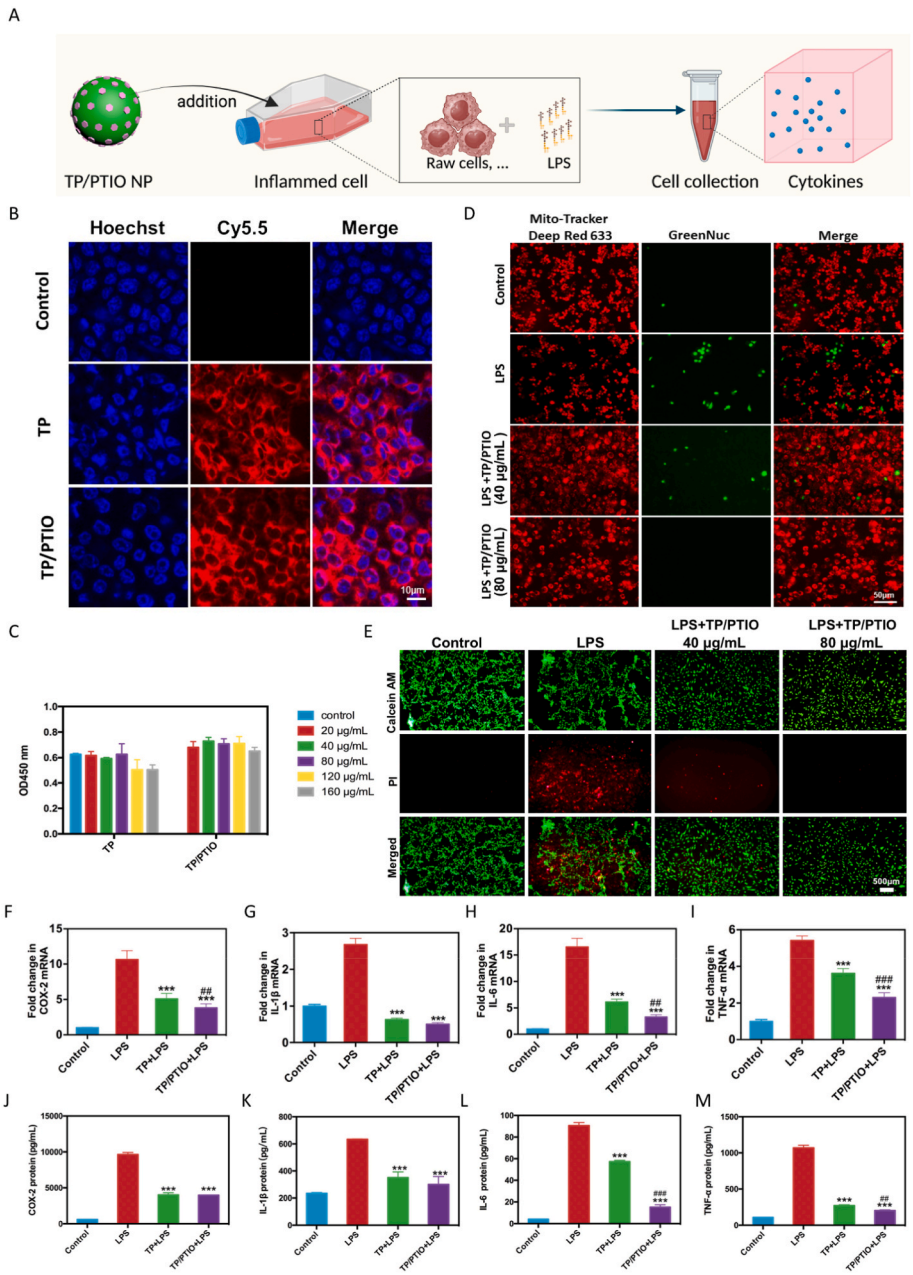

Fig. 2. Anti-inflammatory behaviour of TP/PTIO NPs *in vitro*. (A) Schematic diagram for the *in vitro* experiments. (B) Distribution of TP/PTIO NPs in Raw 264.7 cells. (Blue: nucleus stained with Hoechst 33342. Red: NPs with Cyanine5.5 amine labeling). (C) The cytotoxicity of TP and the TP/PTIO NPs. *P < 0.05, **P < 0.01 relative to the control group. (D) Apoptosis of cells as was determined by Caspase 3/7 GreenNuc staining (green) and live cells by mito-tracker deep red staining (red). (E) Live and dead staining of Raw 264.7 cells with TP/PTIO NPs treatment. (Green: stained with calcein AM; red: stained with PI). (F–I) The mRNA expression and protein production (J–M) of the proinflammatory cytokines COX-2, IL-1β, IL-6, and TNF-α in Raw 264.7 cells after treatment. *P < 0.05, **P < 0.01, and ***P < 0.001 relative to the LPS group. #P < 0.05 compared to the TP + LPS group.

TP and TP/PTIO NPs treatment, and TP/PTIO NPs exerted a slightly more significant ROS scavenging ability compared to TP NPs. ROS play various roles in activating various signaling pathways, among which NF-κB is one of the most important signaling cascades as NF-κB target genes attenuate ROS to prevent hyperinflammation and promote survival and proliferation [57]. In addition, as NF-κB is the major catabolic signaling pathway associated with the pathogenesis of OA [58], we next determined whether TP/PTIO NPs protects cells by downregulating ROS/NF-κB signaling pathway. As shown in Fig. 3I–L, LPS significantly upregulated the expression of NF-κB signaling associated genes, including P50, P65, IκB-α, and IKKβ, while TP and TP/PTIO NP supplementation clearly promoted an anti-inflammatory response to downregulate the above genes, suggesting a significant anti-inflammatory function of TP/PTIO NPs. The protein production of P50, P65, IκB-α, p-IκB-α, p-IKKβ, and COX-2 was also verified by WB, which corresponded to the changes in gene expression levels (Fig. 3M–T).

2.4. NO scavenging and iNOS/NO/caspase-3 signaling regulation in vitro

NO is another important source of stress and apoptotic factors that initiates damage to the knee joint [59]. Chondrocyte is the major cell type in cartilage. Cartilage degeneration due to cell inflammation and apoptosis is the main hallmark of OA, and chondrocytes within the cartilage respond to inflammatory mediators, and regulate matrix production and degradation. For this point, chondrocyte is an ideal cell

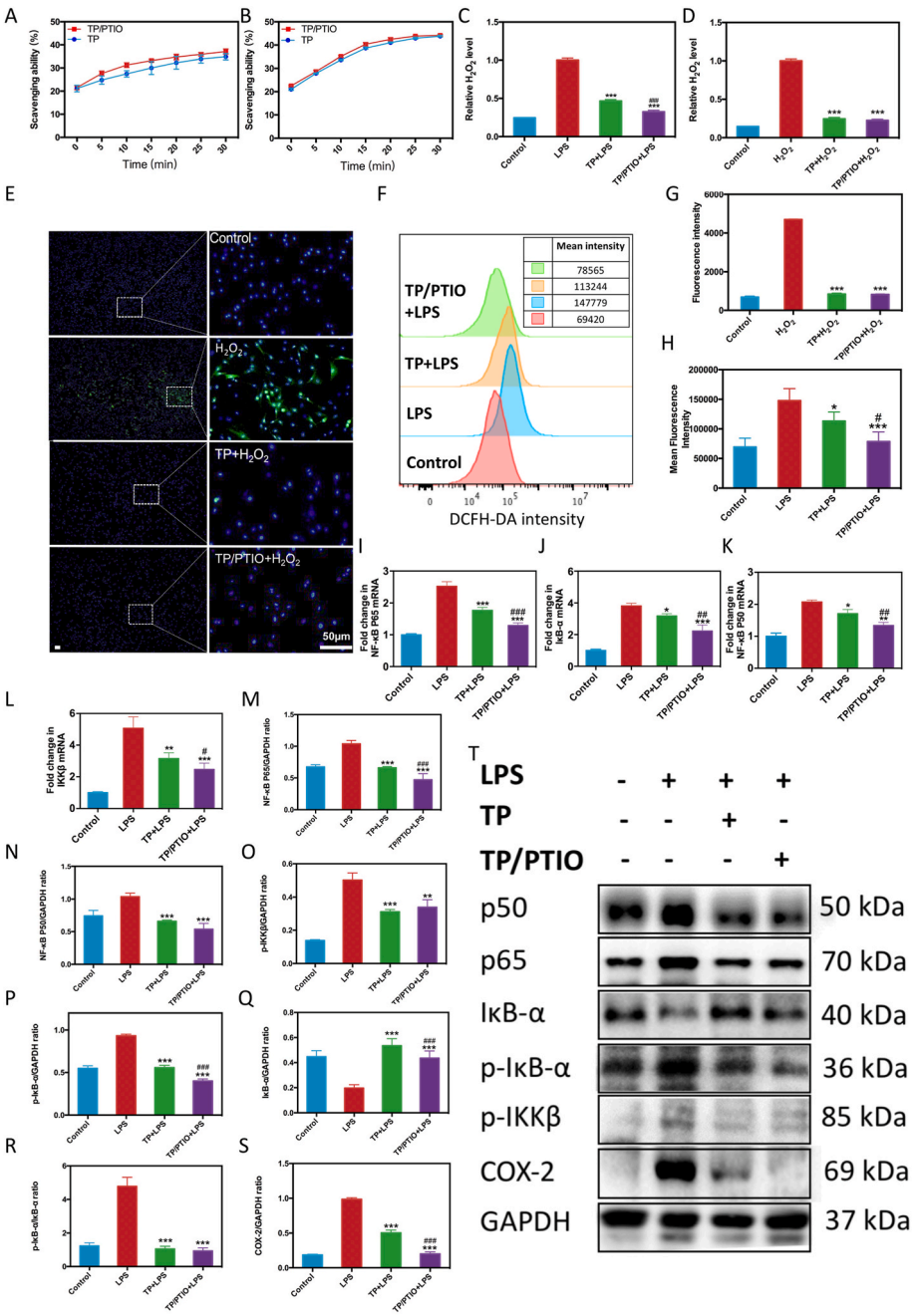

Fig. 3. ROS-scavenging behaviours of NPs and ROS/NF-κB signaling pathways *in vitro*. (A–B) DPPH and ABTS radical scavenging activities of NPs. (C) Relative H_2O_2 concentration in Raw 264.7 cells after LPS stimulation. ***P < 0.001 compared to the LPS group. ###P < 0.001 compared to the TP + LPS group. (D) Relative H_2O_2 concentration in Raw 264.7 cells after ROS stimulation. ***P < 0.001 compared to the LPS group. (E) Raw cells were incubated with H_2O_2 for 4 h, after which TP and the TP/PTIO NPs were added (80 μg/mL) and incubated for 48 h. ROS generation was detected by ROS assay and visualized under a confocal laser microscope (green: stained with DCFH-DA, indicating the level of cellular ROS; blue: stained with Hoechst 33342, indicating the location of the nucleus). The fluorescence intensity and (G) relative H_2O_2 concentration in Raw cells were determined. P < 0.001 relative to the H_2O_2 group. (F) and (H) ROS enriched Raw cells stained with DCFH-DA were further quantified using flow cytometry. *P < 0.05, and ***P < 0.001 relative to the LPS group. #P < 0.05 compared to the TP + LPS group. NF-κB signaling pathway-associated IKKβ, P50, P65, and IκB-α gene expression (I–L) in Raw 264.7 cells after LPS treatment was quantified by RT–qPCR. *P < 0.05, **P < 0.01, and ***P < 0.001 relative to the LPS group. #P < 0.05 compared to the TP + LPS group. (M–T) NF-κB signaling associated protein expressions were further verified by WB.

model for researches on NO associated apoptosis in OA [60,61].

To determine the NO scavenging ability of TP/PTIO NPs, mouse chondrocytes were incubated with sodium nitroprusside (SNP, an NO donor, 100 μM) for 4 h, after which TP or TP/PTIO NPs were added, and mitochondrial membrane damage was evaluated after 24 h using JC-1 staining. For TP/PTIO NPs, as TP scavenges the nitrite generated by carboxy-PTIO reaction, the nitrite concentration decreased significantly after TP/PTIO NPs supplementation (Fig. S9). JC-1 is a fluorescent probe for the detection of mitochondrial membrane potential. When cell is healthy, the mitochondrial membrane is high, JC-1 aggregates in the matrix of mitochondria to form polymers (J-aggregates) which produce red fluorescence. When the membrane potential is low due to damage or apoptosis, JC-1 presents as a monomer (green fluorescence) as it cannot accumulate in the mitochondrial matrix. TP/PTIO NPs effectively

inhibited the decrease in the mitochondrial membrane potential caused by SNP, a NO donor, and restored the mitochondrial membrane potential to the level of the control group (Fig. 4A). At the applied concentration, SNP did not affect chondrocyte viability (Fig. S7). The mitochondrial membrane damage was further evaluated by a Caspase3/7 activity and mitochondrial membrane potential detection assay. Apoptotic cells with enhanced GreenNuc Caspase 3 (green) and decreased Mito-Tracker Deep Red 633 (red) staining were further determined by fluorescence microscopy and quantified using flow cytometry (Fig S8, 4B-C), which demonstrated similar results as the JC-1 staining assay that TP/PTIO NPs effectively inhibited the decrease in the mitochondrial membrane potential caused by SNP. TP and TP/PTIO NPs at the concentrations applied did not affect chondrocytes proliferation over time (Fig. 4F). TP and TP/PTIO NPs also protect chondrocytes by upregulating the expression of the bone-forming genes COL-II and Aggrecan, which are two major components of the cartilage extracellular matrix (ECM), and downregulating the expression of bone loss-associated A disintegrin and metalloproteinase with thrombospondin motif (ADAMTS) and matrix metalloproteinase-13 (MMP-13) (Fig. 4G–J), suggesting a potential anti-inflammatory effect of TP/PTIO NPs. TP/PTIO NPs demonstrated a stronger protective effect than TP NPs, suggesting that carboxy-PTIO released from TP/PTIO NPs effectively inhibited mitochondrial membrane damage. The NO signaling pathway-associated genes encoding iNOS, MMP-13, and Caspase-3 were over-activated in mouse chondrocytes after LPS stimulation but were inhibited by TP and TP/PTIO NPs (Fig. 4J–L), especially TP/PTIO NPs, in mouse chondrocytes, suggesting that carboxy-PTIO released by TP/PTIO could inhibit the cellular inflammation induced by LPS by inhibiting the iNOS/NO/Caspase-3 signaling pathway. Overall, the TP/PTIO NPs exhibited synergistic inhibition of cellular inflammation via dual ROS and NO scavenging.

2.5. The anti-inflammatory behaviours of hydrogel in vivo

OA causes damage to the articular cartilage and underlying bone. Therapy for OA are mainly intra-articular drug delivery which increases local bioavailability, reduces systemic exposure, causes fewer adverse events, and reduce cost. Hyaluronic Acid (HA), glucocorticoids, and promising drug delivery systems such as liposomes vesicle systems are used for intra-articular treatments [62,63]. HA and glucocorticoids can provide clinically meaningful benefits to an appreciable number of patients. However, the high cost, limited half-life, and unclear effectiveness of HA and glucocorticoids have raised concerns over their use in OA [64]. Glucocorticoid administration also found to increase the risk of cartilage volume loss and postoperative infection in patients having total knee arthroplasty [65]. Liposomes as promising drug vesicle systems are known to possess properties such as site-targeting, sustained or controlled release. However, most of the liposome system are known to be unstable by non-covalent interactions, causing leakage and fusion of encapsulated drug/molecules. Besides, liposomes are generally with high cost, short half-life, and low solubility. As natural products derived TP/PTIO NPs are with low cost, sustained drug release capacity, satisfying biocompatibility and easy to manufacture, we applied the NPs to mice with OA to determine if positive therapeutic effects were present. To achieve more lubricated and release controlled *in vivo* friendly materials for OA therapy, a TP/PTIO NP-based injectable hydrogel was designed by mixing TP/PTIO NPs with 4-arm-PEG-SH (Fig. 5A). The viscosity, gelation and drug release capacity of the TP/PTIO + PEG hydrogel was determined first (Figs. S1, S2, S5 and 5B). The intersection of storage modulus and loss modulus of 2.5, 5, 10, 20 mg/mL hydrogels occur in 1300, 550, 400, 250 s, respectively, and this intersection represents the time point at which the solution transitions to gel. The gelation time correlated with the concentration of TP/PTIO NPs (Fig. 5B), as an increase in the TP/PTIO NP ratio led to a shortened hydrogel formation time due to an increase in crosslinking sites. A final TP/PTIO NP concentration of 10 mg/mL was selected for reaction with 50 mg/mL 4-arm-PEG-SH with a gelation time of 400 s, which was adequate and suitable for *in vivo* injection for subsequent animal experiments [66]. An OA animal model was established by injecting 6 μL of papain (4 %, m/v) solution into the knee joint cavity of 8-week-old C57BL/6 mice, as papain-induced OA animal models have been widely used for *in vivo* OA assessment [67]. An OA model with increased perforation, subchondral bone deterioration and enlarged marrow cavities was deemed successful. After 14 days of maintenance, successful OA mice were injected with 10 μL of PBS (group PBS), HA (group HA), TP NPs (group TP), PTIO (group PTIO), TP/PTIO NPs (group TP/PTIO), or TP/PTIO + PEG hydrogel (group TP/PTIO + PEG), respectively. HA was adapted as a positive control group for referring. The detailed treatment strategy was illustrated in Fig. 5A.

Mouse body weights were taken every 2 days, all mice were sacrificed 2 weeks later, and the knee joints were collected for analysis. No significant body weight changes were observed among all tested groups (Fig. S10). The NPs demonstrated an ideal biocompatibility in mice as was demonstrated by hemolysis assay, and HE staining of heart, liver, spleen, lung and kidney (Fig. S11). The Osteoarthritis Research Society International (OARSI) score, a classic evaluation system, was adapted to evaluate cartilage damage in the tibial plateau [68]. All groups treated with NP- or NP-based hydrogels had lower OARSI scores, with the TP/PTIO + PEG hydrogel decreasing the OARSI score most significantly (Fig. 5C). There's a significant change in TP/PTIO group compared to TP group ($p = 0.0222$), and TP/PTIO group compared to PTIO group ($p = 0.0011$). Damage to knee joint cartilage lesions and cartilage substructures was examined after sacrifice via micro-CT (Fig. 5D), and relative parameters were manually segmented and analyzed (Fig. 5E–H). Injection of papain solution caused significant cartilage and subchondral bone destruction (in the PBS group), while the application of the TP/PTIO + PEG hydrogel had the greatest ability to improve the following bone destruction-associated parameters (Fig. 5D–H): the ratio of bone volume to total tissue volume (BV/TV, from 35.67 % to 66.25 %), the ratio of bone surface area to bone surface (BS/BV, from 40.57 % to 27.04 %), the trabecular thickness (Tb.th, from 0.137 mm to 0.186 mm), and the trabecular separation of subchondral bone in condyles (Tb. Sp, from 0.151 mm to 0.099 mm), suggesting that the prepared hydrogel was an ideal agent for OA-related bone regeneration. BV/TV reflects changes in bone volume. BV/TV is the most important parameter in the evaluation of bone changes using microCT. In this study, similar trends were present in the BV/TV (ratio of bone volume to total tissue volume) data that TP/PTIO + PEG demonstrated the best therapeutic effects in OA. There's a significant change in TP/PTIO group compared to TP group ($p = 0.0017$), and TP/PTIO group compared to PTIO group ($p < 0.0001$). There is not much difference between the TP, PTIO and TP/PTIO groups in the BS/BV (represents the area of bone tissue per unit volume), Tb.Sp (represents the average width of the medullary cavity between traceculae), Tb.Th (represents the average trabecular thickness of the phalange) changes. This may attribute to the fact that NPs or Carboxy-PTIO not in a hydrogel form may degrade faster than the hydrogel. The *in vivo* biosafety and tissue regeneration ability of the TP/PTIO + PEG hydrogel were verified by histological staining (Fig. S11). All the mice treated with NPs or hydrogels had an improved prognosis compared with that of the PBS nontherapeutic group according to the histological staining results. Among all the groups that received NP or hydrogel therapy, the TP/PTIO + PEG combination treatment strategy evidently attenuated the histologic deterioration (including proteoglycan and collagen degradation) caused by papain treatment. Similarly, those that received TP/PTIO + PEG hydrogel therapy exhibited the least loss of proteoglycans and a reduced thickness of knee cartilage, as illustrated by safranin O/fast green staining (Fig. 5I).

2.6. Mechanism verification in vivo

In OA mice, significant suppression of upregulated NF-κB and NO

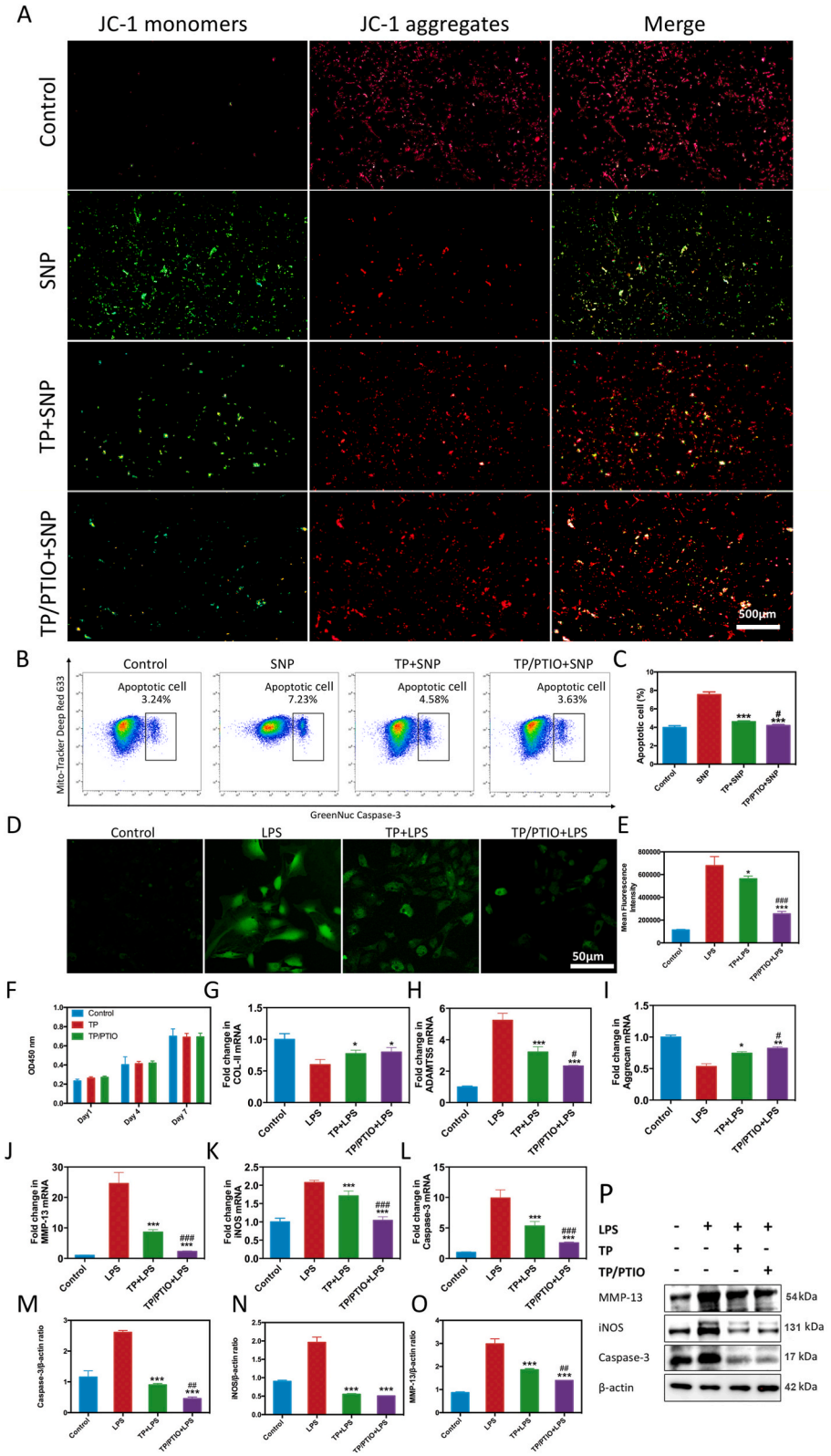

(caption on next page)

Fig. 4. NO-scavenging of the TP/PTIO NPs and iNOS/NO/Caspase-3 signaling pathways *in vitro*. (A) Chondrocytes were incubated with sodium nitroprusside (SNP) for 4 h, after which TP or TP/PTIO NPs were added for 24 h, after which the cell mitochondrial membrane potential was determined by JC-1 staining, and visualized via confocal laser microscopy. Red: high potential; green: low potential; orange: colocalization. (B–C) Apoptotic cells with cell mitochondrial membrane potential changes were stained with GreenNuc Caspase 3 and Mito-Tracker Deep Red 633, and the amount was quantified using flow cytometry. Chondrocytes after LPS treatment were stained with NO probe (DAF-FM DA) and (D) visualized under confocal microscopy, (E) the fluorescence was quantified using flow cytometry. (F) The cell viability of chondrocytes treated with TP/PTIO and TP NPs after 1, 4, and 7 days was determined by the CCK-8 test. (G–I) The effects of TP/PTIO NPs on the expression of bone formation-related genes COL-II, Aggrecan, and ADAMTS5 induced by LPS were determined via qPCR. (J–L) The inhibitory effects of TP/PTIO NPs on iNOS/NO/Caspase-3 signaling pathway-associated gene overexpression of MMP-13, iNOS, and Caspase-3 in mouse chondrocytes were quantified via RT–qPCR. (M – P) MMP-13, iNOS and Caspase-3 protein expression was quantified via WB. *P < 0.05, **P < 0.01, and ***P < 0.001 relative to the LPS group. #P < 0.05, ##P < 0.01, ###P < 0.001 compared with the TP + LPS group.

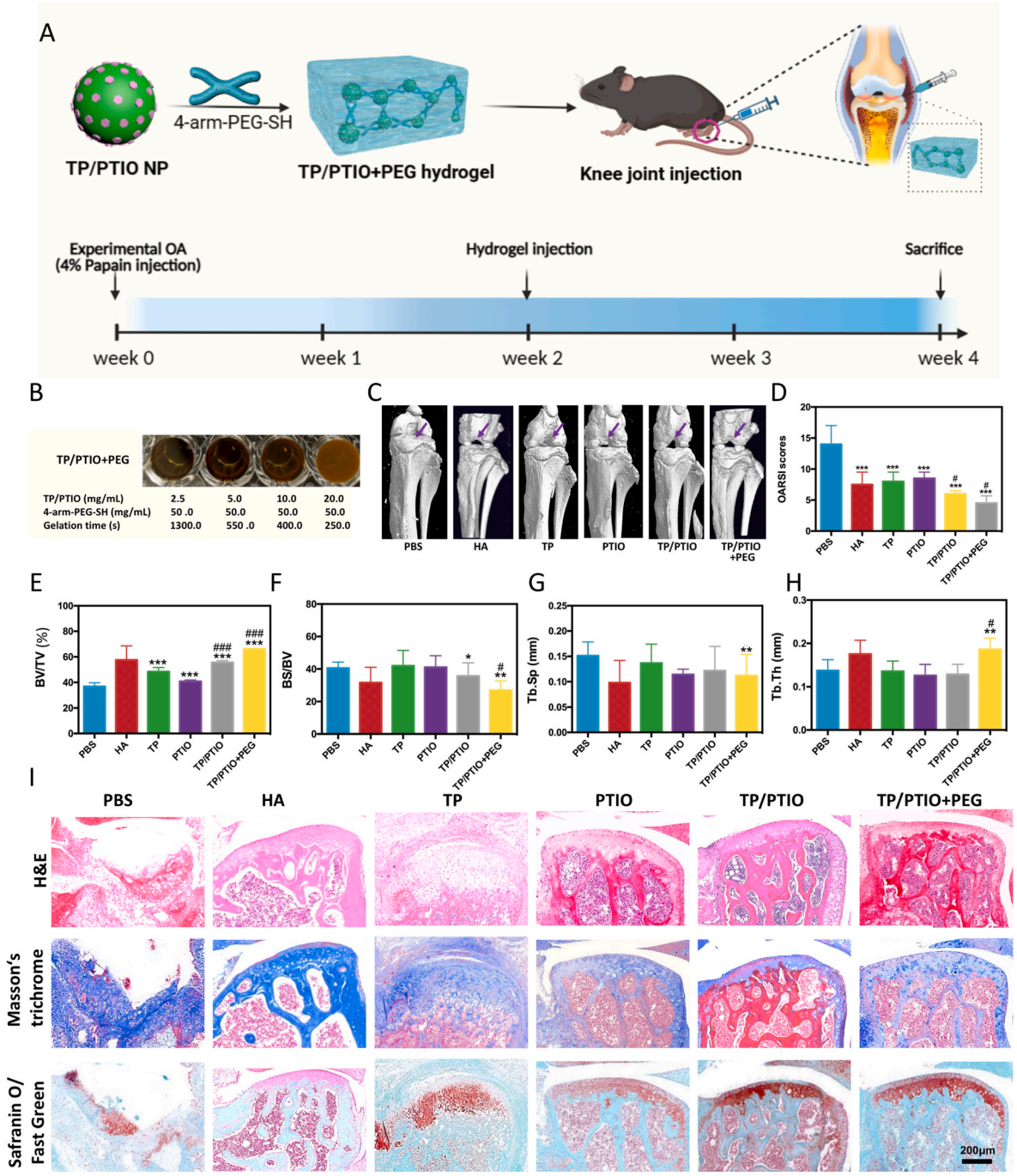

Fig. 5. Anti-inflammatory behaviour of hydrogel in OA mice. (A) Schematic illustration of the *in vivo* animal experiment set up. (B) TP/PTIO + PEG gelation time. (C) OARSI scores and (D) Micro-CT images of the mice in the groups. Subchondral bone physiological condition associated parameters (E–H) were measured. *P < 0.05, **P < 0.01, and ***P < 0.001 compared to the PBS group. #P < 0.05 relative to the TP therapy group. ##P < 0.01, ###P < 0.001 compared to TP group. (I) H&E, Masson's trichrome, and safranin O/fast green staining of knee joints after treatment. Scale bar: 200 μm.

signaling markers, including p65, iNOS, MMP-13, and activated Caspase-3, was observed after treatment with the TP/PTIO + PEG hydrogel according to the immunofluorescence staining results (Fig. 6A), which was in accordance with the *in vitro* gene expression changes in cells. Cartilage ECM-associated markers were also evaluated by immunohistochemistry (IHC), as OA is generally characterized by degradation of the ECM. As shown in Fig. 6B, TP/PTIO + PEG hydrogel injection induced the elimination of the proinflammatory proteins MMP-13 and ADAMTS5, and an increase in the protein production of collagen II and aggrecan, which are major components of the ECM, was

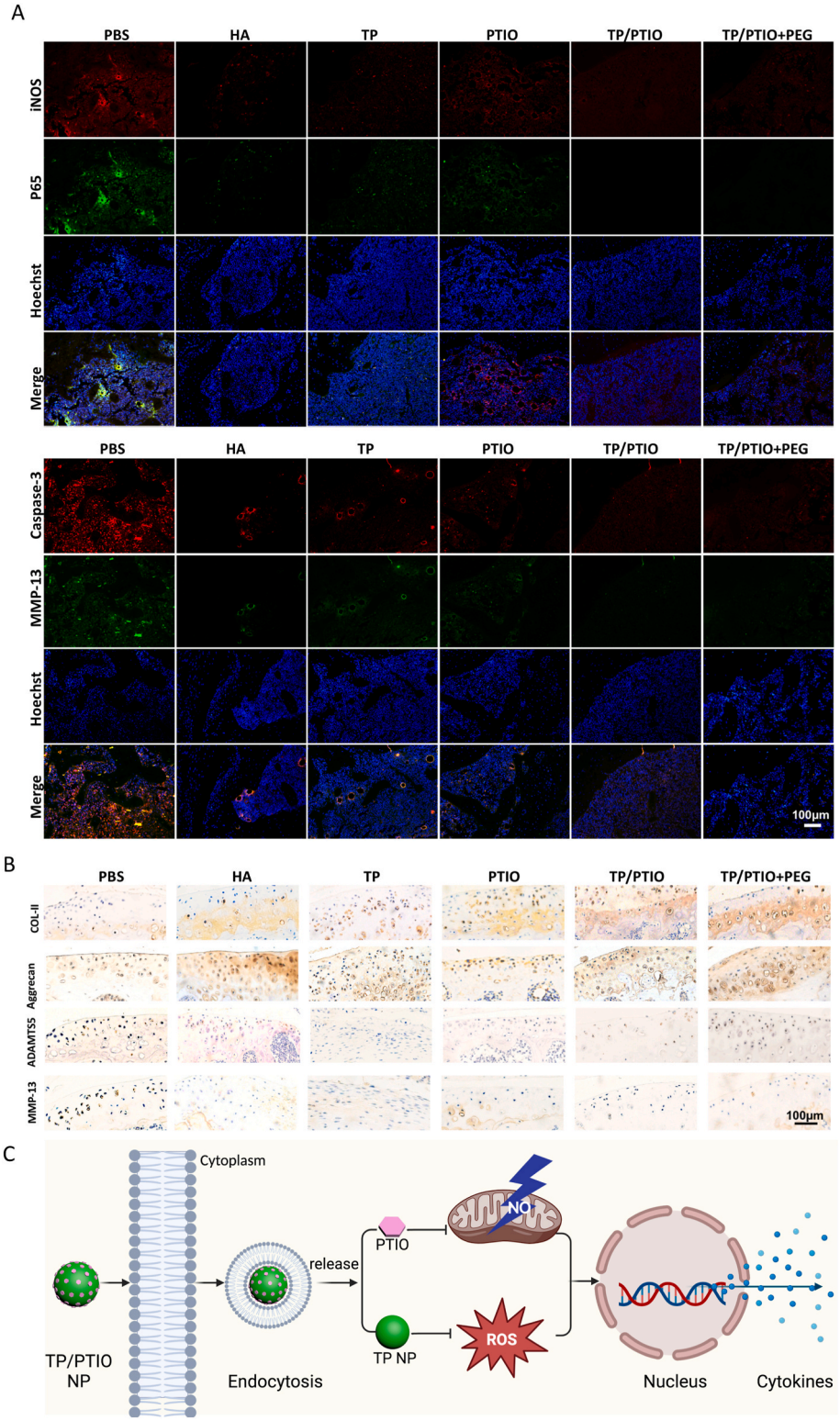

Fig. 6. Dual ROS- and NO-scavenging of the hydrogel *in vivo*. (A) Immunofluorescence microscopy was used to observe the protein expression of p65, iNOS, MMP13 and activated Caspase-3. Scale bar: 100 μm. (B) Immunohistochemistry was used to observe collagen II (COL-II), ADAMTS5, MMP13, and aggrecan protein localization in OA. Scale bar: 100 μm. (C) Proposed signaling pathways involved.

observed. Overall, the acid-responsive release of TP and carboxy-PTIO from the NP system in response to OA microenvironmental pH efficiently prevented cartilage inflammation and damage via ROS/NF-κB and iNOS/NO/Caspase-3 signaling pathways, providing novel conditioned treatment strategies for OA. The proposed signaling pathways are illustrated in Fig. 6C.

3. Conclusion

In summary, we identified a low-cost and acid-responsive smart TP/PTIO + PEG hydrogel system for OA treatment. The TP/PTIO + PEG hydrogel was injectable, highly biocompatible, and possessed dual ROS- and NO-scavenging abilities. TP/PTIO NPs and TP/PTIO + PEG conditionally released TP and carboxy-PTIO under acidic conditions similar to those in the OA microenvironment and protected chondrocytes and innate immune cells from damage caused by ROS and NO by regulating the ROS/NF-κB and iNOS/NO/caspase-3 signaling pathways and controlling cartilage inflammation via similar mechanisms in OA mice. This system may provide insight into the exploration of novel therapeutic biomaterials for OA therapy.

4. Materials and methods

4.1. Materials

Catechol (99 %) was obtained from J&K Chemical Ltd. (China). Tea polyphenols (70 %) containing epicatechin, epigallocatechin, epicatechin gallate, and epigallocatechin gallate were obtained from Wuxi Taiyo Green Power Co., Ltd. (China) [69]. Sodium nitroprusside (SNP) and Hoechst 33342 were obtained from Sigma–Aldrich (USA). 4-arm--PEG-SH was synthesized by Ponsure Biotechnology TM. DMEM and FBS were purchased from Gibco (USA). PBS, methanol and TBST were acquired from ServiceBio Co., Ltd. (China). Horseradish peroxidase (HRP, >300 unit/mg) was from Aladdin Biochemical Technology Co., Ltd. (China). Carboxy-PTIO, CCK-8 assay kit, and JC-1 staining kit were obtained from Beyotime Biotechnology (China). DPPH (95 %) and hydrogen peroxide (H_2O_2) assay kits were obtained from Solarbio Science & Technology Co., Ltd. (China). ABTS diammonium salt (98 %) was obtained from Macklin Reagent Co., Ltd. (China). H_2O_2 (30 %, m/v) was obtained from Sinopharm Chemical Reagent Co., Ltd. TRIzol reagent for quantitative PCR was obtained from Takara Bio Inc. (Japan).

4.2. Synthesis of TP/PTIO + PEG

Catechol (40 mg) and HRP (2.8 mg) was dissolved in deionized water (79.9 mL), following which 0.1 mL H_2O_2 was added in with stirring for several minutes, and 20 mL TP solution was added to the mixture solution at a concentration of 10 mg/mL. The reaction solution was with continuous stirring for 4 h. The resulting TP NPs were obtained by centrifugation after washing [32]. Using TP NPs as carriers, the nitric oxide (NO) scavenger carboxy-PTIO was loaded onto the surface of the TP NPs through π-π interactions to form TP/PTIO NPs. Finally, the sulfhydryl group in 4-arm polyethylene glycol (4-arm-PEG-SH) reacts with catechol on the surface of the TP/PTIO NPs through a Michael addition reaction. An injectable TP/PTIO + PEG hydrogel was formed after crosslinking.

4.3. Characterization

The TP and TP/PTIO NPs morphology was characterized using transmission electron microscopy (TEM, HF-5000, Hitachi, Japan) at an accelerating voltage of 200 kV. Briefly, TP and TP/PTIO NPs solutions were dropped onto the mica substrate and dried thoroughly before testing. The size and zeta potentials of the TP and TP/PTIO NPs were tested through dynamic light scattering technology using a Zetasizer Nano ZS90 (Malvern, UK). The drug loading of the TP/PTIO NPs was determined via ultraviolet–visible absorption spectroscopy. The FT-IR spectra of the NPs were recorded using a Great 20 Fourier transform infrared spectrometer (Zkray, China). The XPS curves of the NPs were determined using an RBD upgraded PHI-5000C ESCA system (PerkinElmer, USA). The UV–Vis spectra of TP, PTIO and TP/PTIO NPs were obtained with a NanoPhotometer (Implen, Germany).

4.4. Drug release from TP/PTIO NPs or TP/PTIO + PEG

The percentages of carboxy-PTIO released from TP/PTIO at pH 6.0 (OA simulating condition) and 7.4 (physiological condition) as well as the amount of TP monomer released from TP NPs were measured separately by HPLC with an Agilent 1220 Infinity II (Agilent, USA). Briefly, the cumulative release of PTIO or TP monomers from TP/PTIO NPs was measured by placing TP/PTIO NPs or TP/PTIO + PEG hydrogel in dialysis membranes (MW1000) in 50 mL ultrapure H_2O with continuous stirring. The solution (200 μL) was collected at indicated time points and measured using HPLC.

4.5. Rheology measurement of TP/PTIO + PEG hydrogel

The rheology measurement was carried out via a hybrid rheometer (Discovery Hibrid Rheometer-3, TA Instruments, New Castle, DE). A 20-mm parallel plate was used for the measurement. The mixture of TP/PTIO and 4-arm-PEG-SH blended on a Vortex mixer for 10 min. After that the mixture was placed on the parallel plate and was sealed by using silicon oil to prevent evaporation. The measurement was conducted at 37 °C with the strain set as 0.1 % and the angular frequency as 10 rad/s. For the shear-thinning measurement, the viscosity of the hydrogel (1.0 cm^3) was measured along with the shear rate at a strain of 0.1 % and an angular frequency of 10 rad s^{-1}.

4.6. ROS scavenging ability

DPPH Free Radical Scavenging Capacity Assay Kit and T-AOC Assay Kit were used to determine the radical scavenging activities. Briefly, 1,1-diphenyl-2-picrylhydrazine (DPPH, 0.05 mg/mL) was incubated with TP NPs for 30 min in the dark after which the absorbance at 517 nm was determined via ultraviolet–visible absorption spectroscopy. The percentage of TP NPs scavenged was calculated following the manufacturer's protocol. For the T-AOC assay, 2,2-diazide bai-bis (3-ethylbenzodu thizhi azole-6-sulfonic acid) diammonium salt (ABTS+, 0.15 mM) was incubated with TP NPs for 6 min in the dark. The absorbance at 734 nm was determined via UV–visible absorption spectroscopy, and the percentage of ROS scavenged from the TP NPs at various concentrations was calculated.

4.7. Cytocompatibility

Raw 264.7 cells were seeded at a density of 10^4 cells/well and treated with TP or TP/PTIO NPs (20, 40, 80, 120, or 160 μg/mL) overnight, after which the cytotoxicity was measured by the CCK-8 test, the cells apoptosis was determined by staining with calcein AM and propidium iodide and visualized using a fluorescence microscope. To determine the cytotoxicity of NPs to chondrocytes, primary mouse chondrocytes were separated from mice prior to the experiments. Briefly, articular cartilage and rib cartilage from the hind limbs of mice were separated and minced into 0.3–0.5 mm pieces, after which 0.25 % trypsin and 0.02 % type II collagenase were added to digest the tissue into cells for 1–2 h. The separated cells were collected after spinning and subsequently incubated with TP or TP/PTIO NPs for the indicated durations. Cell viability of chondrocytes was determined using CCK-8 assay.

4.8. ROS scavenging assay

Raw 264.7 cells were extracted and incubated with H_2O_2, after which TP and TP/PTIO NPs (80 μg/mL) were added and incubated for another 24 h. Reactive oxygen species generation in cells was detected by a ROS assay and visualized under a confocal laser microscope (green is stained by DCFH-DA, indicating the level of cellular ROS, and blue is stained by Hoechst 33342, indicating the location of the nucleus). The fluorescence in the Raw 264.7 cells was determined by a fluorescence microplate reader, and the H_2O_2 concentration in Raw 264.7 cells was determined with a hydrogen peroxide (H_2O_2) assay kit according to the manufacturer's protocols.

4.9. Cell mitochondrial membrane potential and apoptosis

Cell apoptosis was determined by detecting changes in the cell mitochondrial membrane potential and Caspase 3/7 content. Briefly, mouse chondrocytes were incubated with sodium nitroprusside (SNP), a NO donor, for 4 h, after which TP and TP/PTIO NPs were added and incubated for 24 h. The cell mitochondrial membrane potential of mouse chondrocytes was measured using a JC-1 staining kit (Beyotime, China) and Caspase3/7 activity and mitochondrial membrane potential detection assay kit (Beyotime, China) and visualized via confocal laser microscopy.

4.10. Real-time quantitative PCR

Raw 264.7 cells and mouse chondrocytes were treated with the appropriate stimuli, after which the cells were lysed with TRIzol (Takara, Japan), and cellular RNA was extracted and Reverse transcription of RNA was performed using iScriptTM Reverse Transcription Supermix (Bio-Rad, USA). Cytokine expression was evaluated by real-time qPCR with iTaq Universal SYBR Green Supermix (Bio-Rad). Gene expression relative to that of the housekeeping gene GAPDH was analyzed with the ΔΔCt method [70]. The sequences of the primers used are listed in Table S1.

4.11. Western blot analysis

The cells were lysed, and total protein was extracted with RIPA buffer (Beyotime). The extracted protein was then transferred to nitrocellulose filter membranes (Merck, Germany) and incubated with the following primary antibodies: anti-MMP13 (ab39012; Abcam, USA; 1:1000), anti-cleaved caspase-3 (#9664, Cell Signaling Technology), anti-iNOS (ab15323), anti-COX2 (ab179800), NF-κB P65 (ab16502), NF-κB P50 (ab32360), anti-beta-actin (ab227387), anti-IκB-α (9242; Cell Signaling Technology, USA), anti-phospho-IKKα/β (#2697, Cell Signaling Technology), anti-Phospho-IκBα (2859; Cell Signaling Technology), anti-cleaved PARP-1 (#1674, Cell Signaling Technology) and GAPDH (ab9485). After overnight incubation at 4 °C, the membrane was washed and incubated with HRP-conjugated secondary antibodies (Invitrogen, USA) in an orbital shaker. The protein bands were detected via enhanced chemiluminescence (Epienzyme, China) and analyzed using imageJ.

4.12. Enzyme-linked immunosorbent assay (ELISA)

Raw 264.7 cells were incubated with LPS, after which, the culture supernatant was collected and filtered. ELISA assays for TNF-α (R&D, USA), cleaved IL-1 ß (Biolegend, USA), IL-6 (Biolegend, USA), COX-2 (Abcam, USA) were performed following the manufactures' instructions.

4.13. Nitric oxide detection

As NO is unstable in physiological condition, and is easily oxidized to nitrite (NO_2^-), therefore, changes in NO_2^- concentration are commonly used to represent changes in cellular NO production, and the classical Griess reaction was adapted to determine the NO_2^- concentration [71]. Briefly, the culture supernatant was collected and filtered, after which the content of NO was determined using NO detection assay kit (Solarbio, China) following the manufacture's instruction and measured under OD 550 nm.

Alternatively, Raw 264.7 cells were stimulated with LPS for indicated time, after which the NO probe (Beyotime, China) were added to cells for 30 min and incubated in a 37°C atmosphere. Cells stained with NO were visualized under confocal laser microscopy (ZEISS LSM880, Germany) or quantified using flow cytometry (Agilent NovoCyte, USA).

4.14. H_2O_2 content detection

To determine the sustained ROS scavenge ability of TP NPs and compare the ROS scavenge ability with TP monomer and TP monomer based hydrogel, the above particles were incubated with H_2O_2 at a concertation of 1 mM, 100 μM, 10 μM. The H_2O_2 solution were added every 2 h and the remaining H_2O_2 in the culture media were quantified using a H_2O_2 content detection assay (Solarbio, China) in 30 min following every H_2O_2 addition.

4.15. Flow cytometry

Cells after treated were re-suspended in round bottom polystyrene test tube, and stained with DCFH-DA or NO probe or Caspase3/7 and mito-Tracker kit for 30 min. Cells were analyzed using Agilent NovoCyte (USA) platform after staining.

4.16. Immunofluorescence imaging

Raw 264.7 cells were grown in confocal dish for overnight, after which the cells were conditioned with LPS (100 nm/mL) and treated with TP/PTIO NPs for overnight. The cells were then fixed with 4 % Paraformaldehyde, treated with Triton-X 100 (0.1 %), and subjected to immunofluorescence staining using cleaved PARP-1 primary antibody and Alexa Fluor 488 (ab150081) and visualized using confocal microscopy.

4.17. In vivo OA mouse model

All procedures involving animals were approved by the Institutional Animal Care and Use Committees of Shanghai Tenth People's Hospital (SHDSYY-2022-6290). Briefly, an OA model was established by injecting 6 μL of papain (4 %, m/v) solution into the knee joint cavity of 8-week-old C57BL/6 mice, as papain-induced OA animal models have been widely used for *in vivo* OA assessment [67]. The success of the OA model was evaluated by observing the gait of the mice and scanning the cartilage lesions of the knee joint via micro-CT 7 days after injection. After 14 days, the mice with successful OA in the knee joint were randomly divided into 6 groups and injected with 10 μL of PBS, TP NPs (10 mg/mL), PTIO solution (1 mg/mL), TP/PTIO NPs (10 mg/mL), TP + PEG hydrogel, or the TP/PTIO + PEG hydrogel accordingly. The detailed treatment is illustrated in Fig. 5A. All mice were sacrificed after 2 weeks' hydrogel injection, and knee joints with OA were collected for analysis. Damage to knee joint cartilage lesions and cartilage substructures was examined via micro-CT and histological staining.

4.18. Microcomputed tomography (micro-CT) analysis

OA mice receiving PBS, TP NPs, PTIO solution, TP/PTIO NPs, TP + PEG hydrogel, or the TP/PTIO + PEG hydrogel therapy were sacrificed two weeks later, and the knee joints of the mice were taken out for scanning using a high-resolution micro-CT system (Bruker, Belgium). The scanning data were reconstructed using Analyze 12.0 (PerkinElmer)

with a threshold of 3000/8000 (min/max) to isolate bone tissue in the knee joint.

4.19. Histological staining

Knee joints were fixed with 4 % (w/v) paraformaldehyde for 24 h and decalcified in 10 % (w/v) ethylenediaminetetraacetic acid (EDTA, Beyotime) at 37 °C for 4 weeks. The decalcified samples were subsequently dehydrated, embedded in paraffin, cut into 0.3–0.5 mm sections, and subjected to H&E, Masson's trichrome, and safranin O/fast green stainings according to standard protocols. Anti-NF-κB p65, anti-iNOS, anti-MMP13 and anti-cleaved caspase-3 antibodies were used for immunofluorescence staining. Anti-collagen II, anti-aggrecan, anti-adamts5, and anti-MMP-13 antibodies were used for immunohistochemical staining.

4.20. The biocompatibility of materials in vivo

Mice after treatment were suicides, the blood were collected for hemolysis evaluation, and the heart, liver, spleen, lung, kidney were collected and fixed for HE staining. For hemolysis evaluation, fresh blood was incubated with PBS (negative control), Tx-100 (positive control), and NPs, and incubated for 1 h at 37 °C. Hemolysis ratio were determined under OD540nm and calculated using the following formula: Hemolysis ratio=$(OD_{NPs}-OD_{PBS})/(OD_{Tx\text{-}100}-OD_{PBS})$X100 %.

4.21. Statistical analysis

All the experiments were performed in triplicate, and the results are presented as the means ± SDs. All statistical analyses were performed with GraphPad Prism software 6.0 (San Diego, USA) using Student's *t*-test or one-way analysis of variance (ANOVA). A P value < 0.05 was considered as statistical significant.

Ethics approval and consent to participate

All procedures involving animals were approved by the Institutional Animal Care and Use Committees of Shanghai Tenth People's Hospital (SHDSYY-2022-6290).

All authors are in compliance with all relevant ethical regulations.

CRediT authorship contribution statement

Qinfeng Ding: Writing – original draft, Methodology, Formal analysis. **Yitong Wang:** Writing – review & editing, Methodology, Formal analysis. **Tianyou Wang:** Writing – review & editing, Methodology. **Chengyao Zhang:** Methodology, Writing – review & editing. **Shengbing Yang:** Methodology. **Lu Mao:** Conceptualization, Project administration, Writing – review & editing. **Yiyun Cheng:** Writing – review & editing, Project administration, Conceptualization. **Yiwen Li:** Writing – review & editing, Project administration, Methodology, Investigation. **Kaili Lin:** Writing – review & editing, Supervision, Conceptualization.

Declaration of competing interest

None.

Acknowledgments

This work was supported by the National Natural Science Foundation of China (81901002, 32101094), the Shanghai Sailing Program (19YF1425800), the Postdoctoral Scientific Research Foundation of Shanghai 9th People's Hospital, Shanghai Jiao Tong University School of Medicine (Ding Qinfeng-2021-Scientific Research Foundation), Natural Science Foundation of Chongqing (cstc2021jcyj-msxmX0282, msxmX0498), the China Postdoctoral Science Foundation (2017T100320). Finally, the authors thank Yuan Zhang, Yu Chen for their valuable assistance in the manuscript.

Appendix A. Supplementary data

Supplementary data to this article can be found online at https://doi.org/10.1016/j.bioactmat.2024.09.037.

References

[1] M. Cross, E. Smith, D. Hoy, S. Nolte, I. Ackerman, M. Fransen, L. Bridgett, S. Williams, F. Guillemin, C.L. Hill, L.L. Laslett, G. Jones, F. Cicuttini, R. Osborne, T. Vos, R. Buchbinder, A. Woolf, L. March, The global burden of hip and knee osteoarthritis: estimates from the global burden of disease 2010 study, ARD (Ann. Rheum. Dis.) 73 (2014) 1323–1330.

[2] D.T. F, Reva C. Lawrence, Charles G. Helmick, Lesley M. Arnold, Hyon Choi, Richard A. Deyo, Sherine Gabriel, Rosemarie Hirsch, Marc C. Hochberg, Gene G. Hunder, Joanne M. Jordan, Jeffrey N. Katz, Hilal Maradit Kremers, Frederick Wolfe, National Arthritis Data Workgroup, Estimates of the prevalence of arthritis and other rheumatic conditions in the United States. Part II, Arthritis Rheum. 58 (2008) 26–35.

[3] E.M. Gravallese, G.S. Firestein, Rheumatoid arthritis - common origins, divergent mechanisms, N. Engl. J. Med. 388 (6) (2023) 529–542.

[4] A. Mobasheri, G. Kalamegam, G. Musumeci, M.E. Batt, Chondrocyte and mesenchymal stem cell-based therapies for cartilage repair in osteoarthritis and related orthopaedic conditions, Maturitas 78 (2014) 188–198.

[5] X. Sun, X. Zhen, X. Hu, Y. Li, S. Gu, Y. Gu, H. Dong, Osteoarthritis in the middle-aged and elderly in China: prevalence and influencing factors, Int. J. Environ. Res. Publ. Health 16 (23) (2019) 4701.

[6] S.M. Bierma-Zeinstra, B.W. Koes, Risk factors and prognostic factors of hip and knee osteoarthritis, Nat. Clin. Pract. Rheumatol. 3 (2007) 78–85, 1745-8382 (Print)).

[7] D. Prieto-Alhambra, A. Judge, M.K. Javaid, C. Cooper, A. Diez-Perez, N.K. Arden, Incidence and risk factors for clinically diagnosed knee, hip and hand osteoarthritis: influences of age, gender and osteoarthritis affecting other joints, ARD (Ann. Rheum. Dis.) 73 (2014) 1659–1664.

[8] F.J. Blanco, A.M. Valdes, I. Rego-Pérez, Mitochondrial DNA variation and the pathogenesis of osteoarthritis phenotypes, Nat. Rev. Rheumatol. 14 (2018) 327–340.

[9] Y.A.-O. Lee, H.K. Park, Q.S. Auh, H. Nah, J.S. Lee, H.J. Moon, D.N. Heo, I.S. Kim, I. K. Kwon, Emerging potential of exosomes in regenerative medicine for temporomandibular joint osteoarthritis, Int. J. Mol. Sci. 21 (2020) 1541–1562.

[10] S.J. Scrivani, L.B. Keith Da Fau - Kaban, L.B. Kaban, Temporomandibular disorders, N. Engl. J. Med. 359 (2008) 2693–2705, 1533-4406 (Electronic)).

[11] J. Durham, T.R. Newton-John, J.M. Zakrzewska, Temporomandibular disorders, Br. Med. J. 350 (2015) h1154, 1756-1833 (Electronic)).

[12] Z. Ouyang, T. Tan, C. Liu, J. Duan, W. Wang, X. Guo, Q. Zhang, Z. Li, Q. Huang, P. Dou, T. Liu, Targeted delivery of hesperetin to cartilage attenuates osteoarthritis by bimodal imaging with Gd(2)(CO(3))(3)@PDA nanoparticles via TLR-2/NF-κB/Akt signaling, Biomaterials 205 (2019) 50–63.

[13] J.A. Bolduc, J.A. Collins, R.F. Loeser, Reactive oxygen species, aging and articular cartilage homeostasis, Free Radical Biol. Med. 132 (73–82) (2019).

[14] A.B.B. Jan Bondeson, Shane Wainwright, Clare Hughes, Bruce Caterson, Wim B. van den Berg, The role of synovial macrophages and macrophage-produced mediators in driving inflammatory and destructive responses in osteoarthritis, Arthritis Rheum. 62 (2010) 647–657, 1529-0131 (Electronic)).

[15] N. A, J. Martel-Pelletier, J.P. Pelletier, Cytokines and their role in the pathophysiology of osteoarthritis, Front. Biosci. (Online): J. Vis. Literacy 4 (1999) D694–D703.

[16] F. Berenbaum, Osteoarthritis as an inflammatory disease (osteoarthritis is not osteoarthrosis!), Osteoarthritis Cartilage 21 (2013) 16–21.

[17] G. Katona, Osteoarthritis–an inflammatory disease? Int. J. Tissue React. 6 (1984) 453–461.

[18] J.D. Florence Legendre, Jean-Pierre Pujol, Patrick Bogdanowicz, JAK/STAT but not ERK1/ERK2 pathway mediates interleukin (IL)-6/soluble IL-6R down-regulation of Type II collagen, aggrecan core, and link protein transcription in articular chondrocytes. Association with a down-regulation of SOX9 expression, J. Biol. Chem. 278 (2003) 2903–2912.

[19] D.J. R Studer, M. Stefanovic-Racic, P.D. Robbins, C.H. Evans, Nitric oxide in osteoarthritis, Osteoarthritis Cartilage 7 (1999) 377–379.

[20] J.S.P. Kristen M Clements, Mark G. Chambers, Denise M. Visco, A Robin Poole, Roger M. Mason, Gene deletion of either interleukin-1beta, interleukin-1beta-converting enzyme, inducible nitric oxide synthase, or stromelysin 1 accelerates the development of knee osteoarthritis in mice after surgical transection of the medial collateral ligament and partial medial meniscectomy, Arthritis Rheum. 48 (2003) 3452–3463.

[21] S.D.C. Robert Goggs, Gundula Schulze-Tanzil, Mehdi Shakibaei, Ali Mobasheri, Apoptosis and the loss of chondrocyte survival signals contribute to articular cartilage degradation in osteoarthritis, Vet. J. 166 (2003) 140–158. London, England: 1997.

[22] D.R.B.A.J. Farrell, R.M. Palmer, S. Moncada, Increased concentrations of nitrite in synovial fluid and serum samples suggest increased nitric oxide synthesis in rheumatic diseases, ARD (Ann. Rheum. Dis.) 51 (1992) 1219–1222.

[23] B.F. A LeGrand, C. Fink, D.S. Pisetsky, J.B. Weinberg, T.P. Vail, F. Guilak, Interleukin-1, tumor necrosis factor alpha, and interleukin-17 synergistically up-regulate nitric oxide and prostaglandin E2 production in explants of human osteoarthritic knee menisci, Arthritis Rheum. 44 (2001) 2078–2083.
[24] J. Zhang, Y. Fu, P. Yang, X. Liu, Y. Li, Z. Gu, ROS scavenging biopolymers for anti-inflammatory diseases: classification and formulation, Adv. Mater. Interfac. 7 (16) (2020) 2000632.
[25] T. Yuan, T. Wang, J. Zhang, P. Liu, J. Xu, Z. Gu, J. Xu, Y. Li, Robust and multifunctional nanoparticles assembled from natural polyphenols and metformin for efficient spinal cord regeneration, ACS Nano 17 (18) (2023) 18562–18575.
[26] T. Wang, Q. Fan, J. Hong, Z. Chen, X. Zhou, J. Zhang, Y. Dai, H. Jiang, Z. Gu, Y. Cheng, Y. Li, Therapeutic nanoparticles from grape seed for modulating oxidative stress, Small 17 (45) (2021) 2102485.
[27] H. Cao, J. Zhu, J. Zhang, L. Yang, X. Guo, R. Tian, H. Wu, Y. Li, Z. Gu, In situ fabrication of robust polyphenolic hydrogels for skin protection and repair, Chem. Mater. 35 (5) (2023) 2191–2201.
[28] T. Yuan, T. Wang, J. Zhang, S. Shi, Z. Gu, Y. Li, J. Xu, Procyanidins boost the neuroprotective effect of minocycline for intracerebral haemorrhage, Adv. Funct. Mater. 33 (49) (2023) 2303379.
[29] Y. Xu, J. Hu, J. Hu, Y. Cheng, X. Chen, Z. Gu, Y. Li, Bioinspired polydopamine hydrogels: strategies and applications, Prog. Polym. Sci. 146 (2023) 101740.
[30] H. Cao, L. Yang, R. Tian, H.X. Wu, Z.P. Gu, Y.W. Li, Versatile polyphenolic platforms in regulating cell biology, Chem. Soc. Rev. 51 (10) (2022) 4175–4198.
[31] P. Yang, Q.Q. Huang, J.H. Zhang, Y.W. Li, H.L. Gao, Z.P. Gu, Natural polyphenolic nanodots for Alzheimer's disease treatment, Adv. Mater. 36 (3) (2023) e2308393.
[32] P. Yang, J. Zhang, S. Xiang, Z. Jin, F. Zhu, T. Wang, G. Duan, X. Liu, Z. Gu, Y. Li, Green nanoparticle scavengers against oxidative stress, ACS Appl. Mater. Interfaces 13 (33) (2021) 39126–39134.
[33] Y.X. Guo, Q. Sun, F.G. Wu, Y.L. Dai, X.Y. Chen, Polyphenol-containing nanoparticles: synthesis, properties, and therapeutic delivery, Adv. Mater. 33 (22) (2021).
[34] D.L. Gan, W.S. Xing, L.L. Jiang, J. Fang, C.C. Zhao, F.Z. Ren, L.M. Fang, K.F. Wang, X. Lu, Plant-inspired adhesive and tough hydrogel based on Ag-Lignin nanoparticles-triggered dynamic redox catechol chemistry, Nat. Commun. 10 (2019).
[35] J. Yeo, J.A.-O. Lee, S. Yoon, W.A.-O. Kim, Tannic acid-based nanogel as an efficient anti-inflammatory agent, Biomater. Sci. 8 (2020) 1148–1159, 2047-4849 (Electronic)).
[36] K.S. Yuka Maegawa, Hiromu Sakurai, Identification of free radical species derived from caffeic acid and related polyphenols, Free Radic. Res. 41 (2007) 110–119.
[37] S.B. Nimse, D. Pal, Free radicals, natural antioxidants, and their reaction mechanisms, RSC Adv. 5 (2015).
[38] B. Xue, J. Song, L. Liu, J. Luo, G. Tian, Y. Yang, Effect of epigallocatechin gallate on growth performance and antioxidant capacity in heat-stressed broilers, Arch. Anim. Nutr. 71 (2017) 362–372.
[39] J.B.G. Paquay, G.R.M.M. Haenen, G. Stender, S.A. Wiseman, L.B.M. Tijburg, A. Bast, Protection against nitric oxide toxicity by tea, J. Agric. Food Chem. 48 (11) (2000) 5768–5772.
[40] Y. Liu, K. Ai, X. Ji, D. Askhatova, R. Du, L. Lu, J.A.-O. Shi, Comprehensive insights into the multi-antioxidative mechanisms of melanin nanoparticles and their application to protect brain from injury in ischemic stroke, J. Am. Chem. Soc. 139 (2017) 856–862.
[41] S. Deng, S. Shi, X. Xia, Effect of plant polyphenols on the physicochemical properties, residual nitrites, and N-nitrosamine formation in dry-fried bacon, Meat Sci. 191 (2022) 108872.
[42] C. Li, H. Li, Q. Wang, M. Zhou, M. Li, T. Gong, Z. Zhang, X. Sun, pH-sensitive polymeric micelles for targeted delivery to inflamed joints, J. Contr. Release 246 (2017) 133–141 (Electronic)).
[43] G. Farr M K, A.M. Bold, M.J. Kendall, P.A. Bacon, Significance of the hydrogen ion concentration in synovial fluid in rheumatoid arthritis, Clin. Exp. Rhwumatol. 3 (2) (1985) 99–104.
[44] E.J. Goetzi, R.I. Rynes, J.S. Stillman, Abnormalities of respiratory gases in synovial fluid of patients with juvenile rheumatoid arthritis, Arthritis Rheum. 17 (4) (1974) 450–454.
[45] W. Tao, J. Wang, W.J. Parak, O.C. Farokhzad, J. Shi, Nanobuffering of pH-responsive polymers: a known but sometimes overlooked phenomenon and its biological applications, ACS Nano 13 (5) (2019) 4876–4882.
[46] Y. Yan, T. Sun, H. Zhang, X. Ji, Y. Sun, X. Zhao, L. Deng, J. Qi, W. Cui, H.A. Santos, H. Zhang, Euryale ferox seed-inspired superlubricated nanoparticles for treatment of osteoarthritis, Adv. Funct. Mater. 29 (4) (2019) 1807559.
[47] J. Zhang, C. Zhao, R. Sheng, K. Lin, X. Wang, S. Zhang, Construction of a hierarchical micro-/submicro-/nanostructured 3D-printed Ti6Al4V surface feature to promote osteogenesis: involvement of Sema7A through the ITGB1/FAK/ERK signaling pathway, ACS Appl. Mater. Interfaces 14 (27) (2022) 30571–30581.
[48] Y. Wang, J. Cui, J. Chen, J. Wan, Y. Liang, M. Qi, X. Wang, L. Zhang, K. Lin, Novel bone tumor cell targeting nanosystem for chemo-photothermal therapy of malignant bone tumors, Chem. Eng. J. 446 (2022) 136905.
[49] M.Y. Ansari, N. Ahmad, T.M. Haqqi, Oxidative stress and inflammation in osteoarthritis pathogenesis: role of polyphenols, Biomed. Pharmacother. 129 (2020) 110452.
[50] J. Shen, Y. Abu-Amer, R.J. O'Keefe, A. McAlinden, Inflammation and epigenetic regulation in osteoarthritis, Connect. Tissue Res. 58 (1) (2017) 49–63.
[51] Y. Ucuncu, N. Celik, C. Ozturk, M. Turkoglu, N. Cetin, N. Kockara, E. Sener, C. Dundar, A. Arslan, H. Dogan, N. Kurt, H. Suleyman, Chondroprotective effects of a new glucosamine combination in rats: gene expression, biochemical and histopathological evaluation, Life Sci. 130 (2015) 31–37.
[52] L. Qiu, Y. Luo, X. Chen, Quercetin attenuates mitochondrial dysfunction and biogenesis via upregulated AMPK/SIRT1 signaling pathway in OA rats, Biomed. Pharmacother. 103 (2018) 1585–1591.
[53] C.I. Ghanem, M.J. Pérez, J.E. Manautou, A.D. Mottino, Acetaminophen from liver to brain: new insights into drug pharmacological action and toxicity, Pharmacol. Res. 109 (2016) 119–131.
[54] E.B.P. Lopes, A. Filiberti, S.A. Husain, M.B. Humphrey, Immune contributions to osteoarthritis, Curr. Osteoporos. Rep. 15 (6) (2017) 593–600.
[55] M. Mashimo, M. Onishi, A. Uno, A. Tanimichi, A. Nobeyama, M. Mori, S. Yamada, S. Negi, X. Bu, J. Kato, J. Moss, N. Sanada, R. Kizu, T. Fujii, The 89-kDa PARP1 cleavage fragment serves as a cytoplasmic PAR carrier to induce AIF-mediated apoptosis, J. Biol. Chem. 296 (2021) 100046.
[56] S. Yan, X. Zeng, Y. Tang, B.F. Liu, Y. Wang, X.A.-O. Liu, Activating antitumor immunity and antimetastatic effect through polydopamine-encapsulated core-shell upconversion nanoparticles, Adv. Mater. Interfac. 31 (2019) e1905825.
[57] M.J. Morgan, Z.G. Liu, Crosstalk of reactive oxygen species and NF-κB signaling, Cell Res. 21 (1) (2011) 103–115.
[58] P. Lepetsos, K.A. Papavassiliou, A.G. Papavassiliou, Redox and NF-κB signaling in osteoarthritis, Free Radic. Biol. Med. 132 (2019) 90–100.
[59] J.J. Poderoso, K. Helfenberger, C. Poderoso, The effect of nitric oxide on mitochondrial respiration, Nitric Oxide 88 (2019) 61–72.
[60] N. Inanc, S. Jousse-Joulin, K. Abacar,. Cimşit Ç, C. Cimşit, M. D'Agostino, E. Naredo, A. Hocevar, S. Finzel, C. Pineda, H. Keen, A. X. Iagnocco, P. Hanova, W. Schmidt, G. Mumcu, L.A.-O. Terslev, G. Bruyn, The Novel OMERACT Ultrasound Scoring System for Salivary Gland Changes in Patients with Sjögren Syndrome Is Associated with MRI and Salivary Flow Rates, (1499-2752 (Electronic)).
[61] C. Huang, B. Zeng, B. Zhou, G. Chen, Q. Zhang, W. Hou, G. Xiao, L. Duan, N. Hong, W. Jin, Single-cell transcriptomic analysis of chondrocytes in cartilage and pathogenesis of osteoarthritis, Gene. Dis. (2024) 101241.
[62] P. Liu, G. Chen, J. Zhang, A review of liposomes as a drug delivery system: current status of approved products, regulatory environments, and future perspectives, Molecules 27 (4) (2022) 1372.
[63] I.A. Jones, R. Togashi, M.L. Wilson, N. Heckmann, C.T. Vangsness Jr., Intra-articular treatment options for knee osteoarthritis, Nat. Rev. Rheumatol. 15 (2) (2019) 77–90.
[64] N.A. Bedard, D.E. DeMik, N.A. Glass, R.A. Burnett, K.J. Bozic, J.J. Callaghan, Impact of clinical practice guidelines on use of intra-articular hyaluronic acid and corticosteroid injections for knee osteoarthritis, J. Bone Jt. Surg. Am. Vol. 100 (10) (2018) 827–834.
[65] T.E. McAlindon, M.P. LaValley, W.F. Harvey, L.L. Price, J.B. Driban, M. Zhang, R. J. Ward, Effect of intra-articular triamcinolone vs saline on knee cartilage volume and pain in patients with knee osteoarthritis: a randomized clinical trial, JAMA 317 (19) (2017) 1967–1975.
[66] S. Zhu, Y. Li, Z. He, L. Ji, W. Zhang, Y. Tong, J. Luo, D. Yu, Q. Zhang, Q. Bi, Advanced injectable hydrogels for cartilage tissue engineering, Front. Bioeng. Biotechnol. 10 (2022).
[67] X. Meng, S. Grad, C. Wen, Y. Lai, M. Alini, L. Qin, X. Wang, An impaired healing model of osteochondral defect in papain-induced arthritis, J. Orthop. Translat. 26 (2021) 101–110.
[68] W. Waldstein, G. Perino, S.L. Gilbert, S.A. Maher, R. Windhager, F. Boettner, OARSI osteoarthritis cartilage histopathology assessment system: a biomechanical evaluation in the human knee, J. Orthop. Res. : Off. Publ. Orthop. Res. Soc. 34 (1) (2016) 135–140.
[69] S. Yoshino, T. Mitoma, K. Tsuruta, H. Todo, K. Sugibayashi, Effect of emulsification on the skin permeation and UV protection of catechin, Pharmaceut. Dev. Technol. 19 (4) (2014) 395–400.
[70] K.J. Livak, T.D. Schmittgen, Analysis of relative gene expression data using real-time quantitative PCR and the 2-ΔΔCT method, Methods 25 (4) (2001) 402–408.
[71] D.H. Lee, G.P. Pfeifer, Mutagenesis induced by the nitric oxide donor sodium nitroprusside in mouse cells, Mutagenesis 22 (1) (2007) 63–67.